

A new high-pressure phase transition in natural Fe-bearing orthoenstatite

JIN S. ZHANG,^{1,*} PRZEMYSŁAW DERA,² AND JAY D. BASS¹

¹Department of Geology, University of Illinois, Urbana, Illinois 61801, U.S.A.

²Center for Advanced Radiation Sources, University of Chicago, Argonne National Laboratory, Argonne, Illinois 60439, U.S.A.

ABSTRACT

Single-crystal X-ray structure refinements have been carried out on natural Fe-bearing orthoenstatite (OEN) at pressures up to 14.53 GPa. We report a new high-pressure phase transition from OEN to a monoclinic phase (HPCEN2) with space group $P2_1/c$, with a density change of $\sim 1.9(3)\%$. The HPCEN2 phase is crystallographically different from low-pressure clinoenstatite (LPCEN), which also has $P2_1/c$ symmetry. Upon release of pressure HPCEN2 reverts to OEN, and the transition pressure is bracketed between 9.96 and 14.26 GPa at room temperature. We find no evidence for a $C2/c$ phase at high pressure. The lattice constants for the new phase at 14.26 GPa are $a = 17.87(2)$, $b = 8.526(9)$, $c = 4.9485(10)$ Å, $\beta = 92.88(4)^\circ$ [$\rho = 3.658(9)$ g/cm³]. Refinement of the new structure indicates rotation of tetrahedral chain as the key characteristic of this transition. This experiment points to the possibility of OEN and HPCEN2 as the stable phases in Earth's upper mantle.

Keywords: Orthoenstatite, high-pressure clinoenstatite, high-pressure phase transition, upper mantle, synchrotron single-crystal X-ray diffraction

INTRODUCTION

Mg-rich, Fe-bearing pyroxene with approximate composition (Mg,Fe)SiO₃ is widely believed to be the second most abundant mineral in Earth's upper mantle. Previous experiments suggest that three polymorphs of (Mg,Fe)SiO₃ are potentially stable under upper mantle conditions: orthoenstatite (OEN) with space group $Pbca$ (Morimoto and Koto 1969), low-pressure clinoenstatite (LPCEN) with space group $P2_1/c$ (Morimoto et al. 1960), and high-pressure clinoenstatite (HPCEN) with space group $C2/c$ (Angel et al. 1992). At high temperature and pressure, OEN is thought to transform to HPCEN between 6–9 GPa, depending on the temperature (Pacalo and Gasparik 1990; Kanzaki 1991; Ulmer and Stadler 2001). HPCEN cannot be quenched to ambient conditions, but transforms to LPCEN (Angel et al. 1992; Kung et al. 2004), which is considered to be the thermodynamically stable phase of (Mg,Fe)SiO₃ at low pressures and $T < 600$ °C (Grover 1972). The phase transition from HPCEN→LPCEN occurs at ~ 8 GPa for MgSiO₃ composition (Angel et al. 1992; Shinmei et al. 1999) and was proposed as a possible explanation for the X discontinuity in deeper part of the uppermost mantle (Woodland 1998; Akashi et al. 2009; Deuss and Woodhouse 2004).

There are several reasons to question the stability of LPCEN and its relevance as a major phase in the crust and upper mantle. The geologic record gives a significant clue, in that natural occurrences of LPCEN are rare, whereas orthopyroxene is a common rock-forming mineral in igneous and metamorphic environments (Anthony et al.). LPCEN forms only under special conditions both in the lab and natural environments, such as rapid quench from high temperature (Smyth 1974; Crawford 1980), under large shear stresses (Coe and Kirby 1975; Frost et al. 1978), in the presence of fluxes or an H₂O-rich environment

(Grover 1972; Ulmer and Stadler 2001; Shiraki et al. 1980; Ito 1975; Grandin de L'Épervier and Ito 1983), or from synthetic samples that contain flux impurities, which may, quite possibly, stabilize the LPCEN structure (Angel et al. 1992; Chopelas 1999; Jacobsen et al. 2010). Moreover, most experiments to date have been performed on Fe-free OEN, whereas the phase relations of natural Fe-Al-Ca-bearing OEN could be different (Angel et al. 1992; Chopelas 1999; Shinmei et al. 1999; Kung et al. 2004; Akashi et al. 2009). The stable form of natural Mg-rich pyroxene under near-surface conditions is thus far from certain. In this paper, we reinvestigate the low-temperature high-pressure phase diagram of (Mg,Fe)SiO₃, in particular the stability of LPCEN and HPCEN.

EXPERIMENTAL METHODS

In situ single-crystal X-ray diffraction (XRD) experiments were carried out at GeoSoilEnviroCARS (GSECARS, Sector13) experimental station 13IDD of the Advanced Photon Source (APS), Argonne National Laboratory (ANL), using natural single-crystal samples of OEN.

Pre-oriented high-quality San Carlos OEN single crystals with chemical composition of (Mg_{1.74}Fe_{0.16}Al_{0.05}Ca_{0.04}Cr_{0.01})(Si_{1.94}Al_{0.06})O₆ (by EMPA analysis), and lattice parameters of $a = 18.268(9)$, $b = 8.821(4)$, $c = 5.197(2)$ Å [$\rho_0 = 3.288(4)$ g/cm³], were polished into plate-like samples (~ 30 μm thickness) with two different orientations that were determined by single-crystal X-ray diffraction.

All high-pressure experiments were performed with a modified 3-pin Merrill-Bassett-style cell with a 90° conical aperture, which provides $\pm 18^\circ$ diffractive X-ray aperture. Rhenium or stainless steel metal gaskets with an initial thickness of 250 μm were pre-indenting to 60 μm using 400 μm culet diamond anvils. A 235 μm diameter hole in the gasket formed the sample chamber. Two plate-like samples (maximum ~ 40 – 50 μm size) with orientations of (010) and (522), and several ruby balls were loaded together in the diamond-anvil cell (DAC) sample chamber. Neon was loaded as a pressure medium to minimize the differential stress using the GSECARS/COMPRES gas loading system (Rivers et al. 2008). Pressure was determined from ruby fluorescence (Mao et al. 1986).

A monochromatic beam with incident energy of 37 keV was focused by a pair of Kirkpatrick-Baez mirrors to a spot size of 3×5 μm. XRD images were collected using a MAR165 charge coupled device (CCD) detector, placed at a sample-to-detector

* E-mail: zhang72@illinois.edu

distance of ~200 mm. During exposures the sample was rotated about the vertical axis (ω) in the range of $\pm 18^\circ$, with a typical exposure time of 0.5 s/ $^\circ$. Diffraction images were collected at three different detector positions, differing by a 70 mm horizontal translation perpendicular to the incident beam. The detector geometry parameters at each detector position were calibrated with CeO₂ diffraction standard. In addition to the full-rotation exposures, a step-scan with 0.5 or 1 $^\circ$ rotation steps was performed at each pressure step, for each of the crystals.

Diffraction images were analyzed using the GSE_ADA/RSV software package (Dera 2007). Because of the high-incident energy and negligible sample thickness, the sample absorption was ignored. Peaks from exposures at the three different detector positions were scaled and merged together. The resulting lists of peaks with corresponding squares of structure factor amplitudes $|F|^2$ and their standard deviations were used for structure solution and subsequent refinement. The high-pressure structure was solved by converting the *Pbca* structure model refined before the transition to the *P2₁/c* setting (translation gleiche sub-group-super-group relation determined with the use of Powder Cell 2.3 program) and refining the resulting model by means of simulated annealing approach, as implemented in the computer program Endeavor (Putz et al. 1999). The model obtained from the Endeavor refinement was then used as a starting point for a conventional least-squares crystal structure refinement using the SHELXL program (Sheldrick 2008). Structure refinement was done using anisotropic displacement parameters for all atoms.

RESULTS

Diffraction data collected at the first pressure point of 6.70 GPa was successfully indexed using the orthorhombic unit cell

of the ambient-pressure orthorhombic *Pbca* phase. With increasing pressure, the *Pbca* structure was confirmed for both samples at 6.70, 11.04, 11.54, and 12.66 GPa. New diffraction peaks appeared when pressure reached 14.26 ± 0.05 GPa, as shown in Figure 1. Diffraction patterns collected from both crystals were consistent and showed the same effect. The new patterns were indexed ab initio (without any initial assumptions about the unit cell), and yielded a primitive monoclinic unit cell with $a = 17.87(2)$, $b = 8.526(9)$, $c = 4.9485(10)$ Å, $\beta = 92.88(4)$ Å. Subsequent analysis of systematic absences indicated the best-fit space group to be *P2₁/c*. As discussed below, the unit cell of the new phase is closely related to that of the original OEN phase.

Upon release of pressure to 9.96 GPa, the *Pbca* orthorhombic structure reappeared, and peaks from the *P2₁/c* structure were absent. Thus, this transition is completely reversible, with the transition pressure P_{tr} bracketed in the range 9.96 and 14.26 GPa. The high-pressure *P2₁/c* phase (HPCEN2) is not quenchable. The rapidity of the transition suggests that kinetic barriers are small, although additional experiments will be required to narrow P_{tr} .

Structural refinements of OEN agree with previous results (Hugh-Jones and Angel 1994). However, the new high-pressure

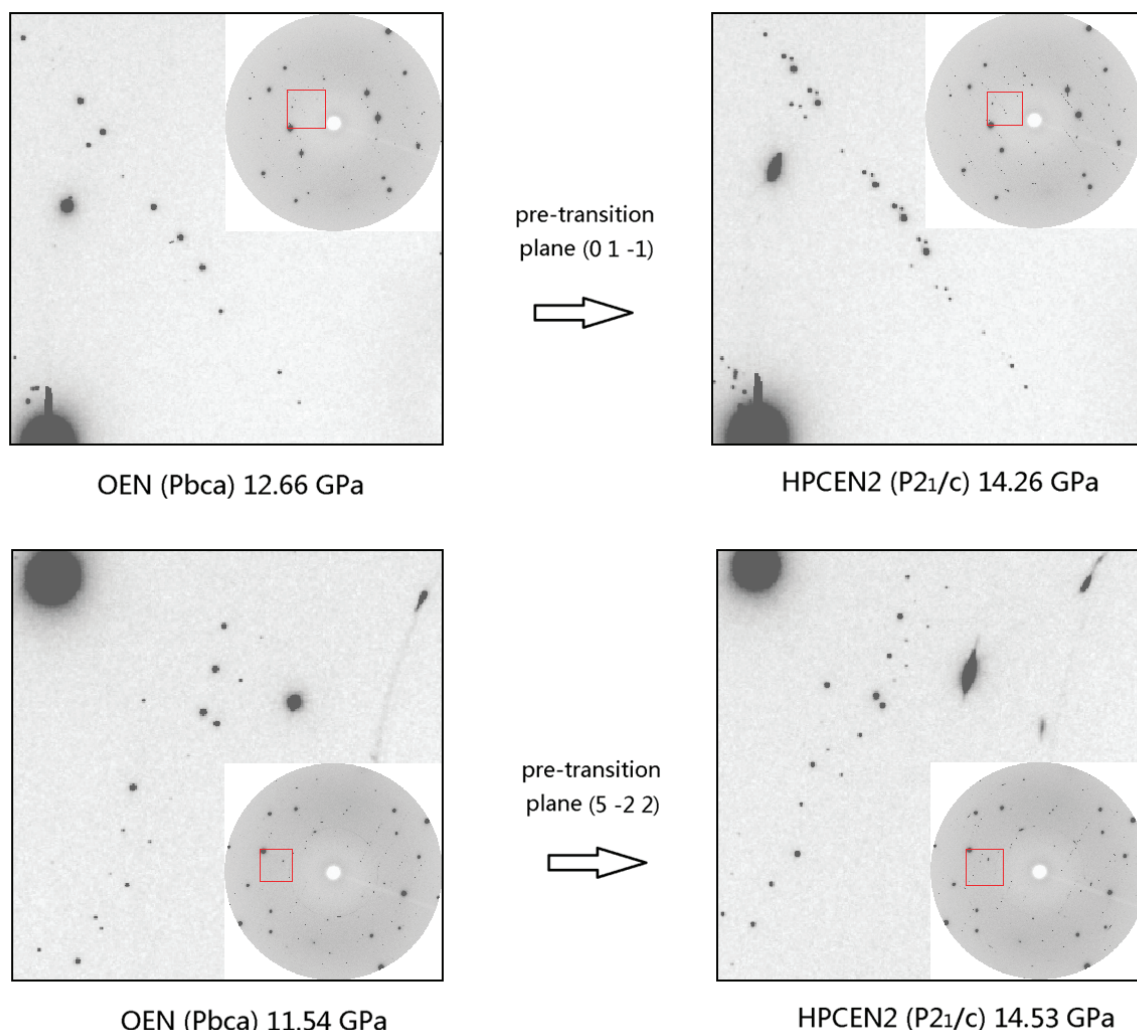


FIGURE 1. Comparison of single-crystal diffraction patterns before and after the OEN-HPCEN2 transition. (Color online.)

phase HPCEN2 could not be refined to either OEN, LPCEN, HPCEN, or any combination of them, although HPCEN2 has the same space group ($P2_1/c$) as LPCEN (Hugh-Jones and Angel 1994; Ohashi 1984; Angel et al. 1992). The unit-cell parameter $\beta = 107.74(2)^\circ$ for the LPCEN phase is much greater than, thus easily distinguished from, that for HPCEN2 [$\beta = 92.88(4)^\circ$, Table 1]. Structural refinement results for HPCEN2 show that half of the tetrahedra in every other tetrahedral layer change from the original O configuration to an S configuration across the OEN→HPCEN2 transition, accompanied by a change in the O3-O3-O3 angle for the A-site Si-O tetrahedra from $160.71(16)^\circ$ to $216.61(77)^\circ$ and $148.44(79)^\circ$ (Fig. 2; Table 2; CIF available¹). This leads to the formation of a novel structure with four symmetrically independent Mg/Fe sites (two originating from M1 and two from M2) and four Si sites, thereby decreasing the symmetry to $P2_1/c$. Using topological I-beam representation of the pyroxene structure, it is apparent that the HPCEN2 structure is topologically much closer to the parent orthoenstatite (OEN) structure (Fig. 3) than the LPCEN or HPCEN structures. The alternating

(+)(+)(-)(-) sequence of octahedral layer stagger is a distinctive signature of the orthopyroxene topology. The new high-pressure phase remains this character although its symmetry decreases to monoclinic—the O to S configuration change of tetrahedral chain is the main characteristic of this transition.

The new phase has the ideal pyroxene structure no.8b of Thompson and Downs (2003). The transition mechanism and transition pressure range is very similar to the calculated transition from OEN to an orthorhombic high-pressure polymorph HP-OEN2 predicted by Jahn (2008). The OEN→HP-OEN2 transition predicted by Jahn (2008) is also characterized by an incomplete O to S configuration change within the tetrahedral layers. It therefore seems possible that a complete O to S configuration change might occur in another higher-pressure phase transition as pressure increase above 15 GPa.

The structure refinements also took into account the Fe/Mg substitution. For the $Pbca$ OEN phase it shows 2.7% Fe in M1 site and 14.7% Fe in the M2 site, whereas for the $P2_1/c$ HPCEN2 phase the four distinct Mg sites showed different Fe percentages: 4, 5, 16, and 12%, (Table 2). For high-pressure in-situ single-crystal refinement of the compositional substitution, considering the very small Z -number contrast between Mg and Fe, the expected uncertainty is around several percent, and the resulting disorder model in both phases is reasonable when compared with EMPA results.

TABLE 1. Crystal data and structure refinement for OEN and HPCEN2.

Sample	OEN ($P = 12.66$ GPa)	HPCEN2 ($P = 14.26$ GPa)
Crystal system, space group	Orthorhombic, $Pbca$	Monoclinic, $P2_1/c$
Unit-cell dimensions	$a = 17.868(8)$ Å $b = 8.491(3)$ Å $c = 5.0565(6)$ Å	$a = 17.87(2)$ Å $b = 8.526(9)$ Å $\beta = 92.88(4)^\circ$ $c = 4.9485(10)$ Å
Volume	$767.2(4)$ Å ³	$753.2(12)$ Å ³
Z , Calculated density	8, 3.589(3) g/cm ³	8, 3.658(9) g/cm ³
Reflections collected/unique	760/254 ($R_{int} = 0.0613$)	530/203 ($R_{int} = 0.0658$)
Data/restraints/parameters	254/0/53	203/0/85
Goodness-of-fit on F^2	1.142	0.878
Final R indices [$I > 2\sigma(I)$]	$R_1 = 0.0357$, $wR_2 = 0.0872$	$R_1 = 0.0465$, $wR_2 = 0.1266$

¹ Deposit item AM-12-050, CIF. Deposit items are available two ways: For a paper copy contact the Business Office of the Mineralogical Society of America (see inside front cover of recent issue) for price information. For an electronic copy visit the MSA web site at <http://www.minsocam.org>, go to the *American Mineralogist* Contents, find the table of contents for the specific volume/issue wanted, and then click on the deposit link there.

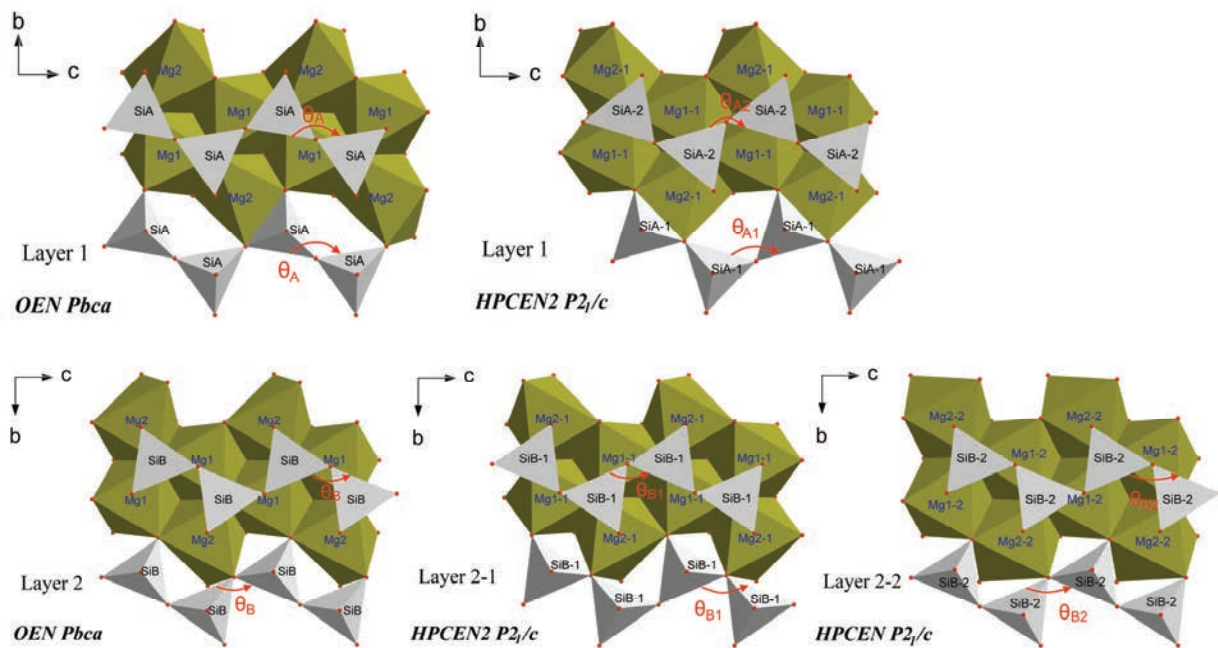


FIGURE 2. Polyhedral illustration of the structural change from OEN ($Pbca$) to HPCEN2 ($P2_1/c$). The O3-O3-O3 angle of the $Pbca$ structure $\theta_A = 160.71(16)^\circ$ (layer 1) changed to $\theta_{A1} = 148.44(79)^\circ$ and $\theta_{A2} = 216.61(77)^\circ$; in layer 2, $\theta_B = 135.44(15)^\circ$ changed to $\theta_{B1} = 131.94(72)^\circ$ and $\theta_{B2} = 133.13(49)^\circ$. (Color online.)

TABLE 2. Atomic coordinates and equivalent isotropic displacement parameters (\AA^2) for OEN and HPCEN2

	Occupancy	<i>x</i>	<i>y</i>	<i>z</i>	U_{eq}
OEN					
Mg1	0.973(7)	0.3762(1)	0.6585(3)	0.8537(3)	0.007(1)
Mg2	0.853(8)	0.3780(1)	0.4790(2)	0.3482(2)	0.009(1)
Fe1	0.027(7)	0.3762(1)	0.6585(3)	0.8537(3)	0.007(1)
Fe2	0.147(8)	0.3780(1)	0.4790(2)	0.3482(2)	0.009(1)
SiA	0.2706(1)	0.3446(2)	0.0331(2)	0.006(1)	0.006(1)
SiB	0.4726(1)	0.3382(2)	0.8052(2)	0.006(1)	0.006(1)
O1a	0.1818(2)	0.3404(5)	0.0201(6)	0.007(1)	0.007(1)
O2a	0.3086(3)	0.5120(5)	0.0287(7)	0.008(1)	0.008(1)
O3a	0.3045(2)	0.2247(5)	-0.1868(6)	0.010(1)	0.010(1)
O1b	0.5630(2)	0.3383(5)	0.8114(5)	0.008(1)	0.008(1)
O2b	0.4333(3)	0.4886(5)	0.6826(6)	0.010(1)	0.010(1)
O3b	0.4444(2)	0.1890(5)	0.6169(6)	0.009(1)	0.009(1)
HPCEN2					
Mg1-1	0.96(3)	0.3759(4)	0.6574(9)	0.8231(11)	0.009(3)
Mg1-2	0.95(3)	0.1254(5)	0.3419(9)	0.3658(12)	0.008(3)
Mg2-1	0.84(3)	0.3826(4)	0.4820(11)	0.3282(11)	0.0116(19)
Mg2-2	0.88(3)	0.1247(4)	0.5275(8)	0.8672(11)	0.009(2)
Fe1-1	0.04(3)	0.3759(4)	0.6574(9)	0.8231(11)	0.009(2)
Fe1-2	0.05(3)	0.1254(5)	0.3419(9)	0.3658(12)	0.008(3)
Fe2-1	0.16(3)	0.3826(4)	0.4820(11)	0.3282(11)	0.0116(19)
Fe2-2	0.12(3)	0.1247(4)	0.5275(8)	0.8672(11)	0.009(2)
SiA-1	0.2716(4)	0.3414(9)	0.0258(11)	0.0258(11)	0.0069(14)
SiA-2	0.2271(4)	0.6572(9)	0.4422(11)	0.4422(11)	0.0092(14)
SiB-1	0.4721(4)	0.3398(7)	0.8079(10)	0.8079(10)	0.0084(14)
SiB-2	0.0249(5)	0.6585(7)	0.3125(11)	0.3125(11)	0.0101(14)
O1a-1	0.1835(10)	0.3414(17)	0.0380(30)	0.0380(30)	0.006(3)
O1a-2	0.3157(10)	0.6630(20)	0.4710(20)	0.4710(20)	0.004(3)
O2a-1	0.3112(8)	0.5080(30)	-0.0120(20)	-0.0120(20)	0.005(3)
O2a-2	0.1871(9)	0.5030(20)	0.5470(30)	0.5470(30)	0.014(3)
O3a-1	0.3046(10)	0.2090(20)	0.8390(30)	0.8390(30)	0.010(3)
O3a-2	0.1968(10)	0.7020(20)	0.1280(30)	0.1280(30)	0.014(3)
O1b-1	0.5637(11)	0.3340(20)	0.8280(30)	0.8280(30)	0.010(3)
O1b-2	0.9370(10)	0.6520(17)	0.3080(30)	0.3080(30)	0.006(3)
O2b-1	0.4368(9)	0.4960(20)	0.6780(20)	0.6780(20)	0.010(3)
O2b-2	0.0619(8)	0.5152(18)	0.1850(20)	0.1850(20)	0.001(2)
O3b-1	0.4447(11)	0.1854(19)	0.6200(30)	0.6200(30)	0.010(3)
O3b-2	0.0534(9)	0.8130(19)	0.1310(20)	0.1310(20)	0.007(3)

Note: U_{eq} is one third of the trace of the orthogonalized U_{ij} isotropic displacement tensor.

DISCUSSION AND CONCLUSION

The increased repulsion between the M2-site cation and A-site Si seems to be a key factor that dominates the topology of pyroxene structures at higher pressure. Indeed, the O to S configuration change tends to provide a more distorted and larger site for the M2 cation, increasing the M2-Si(A) distance and stabilizing the structure. This process is sensitive to the charge and radius of the M2-site cation, making these crucial factors for the topology and symmetry of the high-pressure phase. The stability of different pyroxene structures should thus be sensitive to chemical composition, for example the presence of Fe, Al, Ca, and trace impurities (e.g., Mo, V, Li, etc.). It is therefore plausible that the *P-T* phase diagram of OEN with just 8–10% Fe and minor levels of Al and Ca could be distinct from that of end-member MgSiO_3 .

Angle-dispersive X-ray powder diffraction patterns were calculated based on structural refinements of OEN and HPCEN2, for comparison with HPCEN and LPCEN (Fig. 4). The significant differences in patterns for these phases makes powder diffraction an effective tool for distinguishing the phases of $(\text{Mg,Fe})\text{SiO}_3$.

► **FIGURE 4.** Calculated angle-dispersive powder diffraction patterns of OEN (*Pbca*), HPCEN2 (*P2₁/c*), and comparison with experimental LPCEN (*P2₁/c*) and HPCEN (*C2/c*). (Color online.)

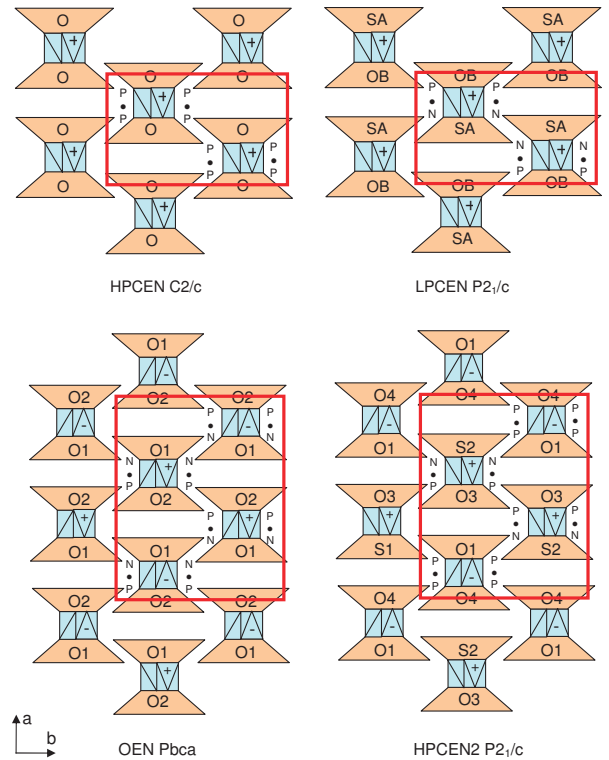
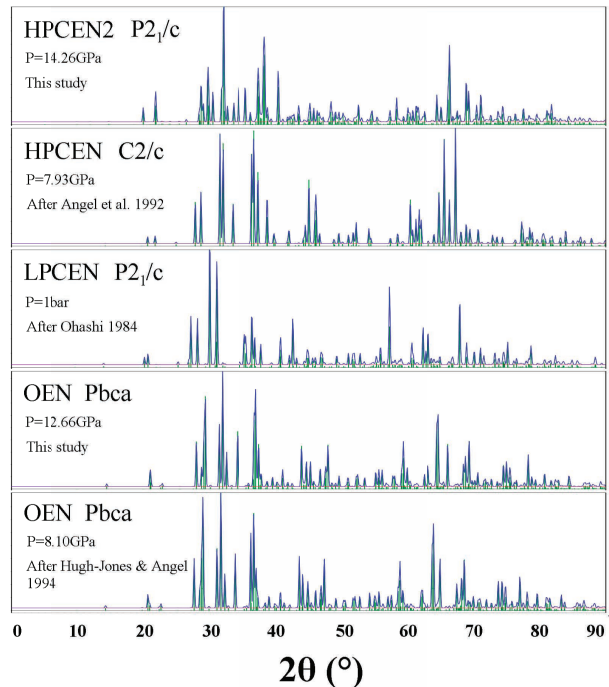


FIGURE 3. I-beam topological representation for $(\text{Mg,Fe})\text{SiO}_3$ polymorphs: OEN (*Pbca*), HPCEN2 (*P2₁/c*), LPCEN (*P2₁/c*), and HPCEN (*C2/c*). Note: P denotes a configuration in which the octahedral and tetrahedral triangular faces point in the same directions within an I-beam, whereas N describes opposite orientations of the two faces. (+) (–) symbols refer to the direction of stagger of the layers respect to right-handed set of crystallographic axes (Papike et al. 1973). (Color online.)



Although some calculations have predicted pure MgSiO₃ OEN to be metastable under ambient conditions (e.g., Yu and Wentzcovitch 2009; Jahn 2008), the Gibbs free energy differences between these two phases are very small and likely within the uncertainties of calculations. Moreover, Ca-poor pyroxene in the mantle likely contains ~10 mol% Fe along with minor Al and Ca, all of which will affect the thermodynamic properties and stability fields of the various possible (Mg,Fe)SiO₃ structures. Calculations that account for Fe and minor elements in OEN will be important for understanding the high-*P-T* phase transitions.

It is worth noticing that Kung et al. (2004) observed anomalous acoustic softening in an ultrasonic study of synthetic polycrystalline MgSiO₃ over a pressure range similar to that covered by our study. Similarly, Lin (2003) observed a significant change in the Raman spectrum between 9.5–10 GPa under room-temperature conditions, and the new spectrum was distinct from that observed for HPCEN with *C2/c* symmetry (Lin 2004). It is entirely possible that the unresolved structures suggested in both of these studies were in fact the HPCEN2 structure characterized in this study.

Our experiments indicate that OEN is likely to be the stable phase of (Mg,Fe)SiO₃ in a dry uppermost mantle. Previous high-temperature room-pressure experiments have already suggested the formation of OEN instead of LPCEN by slow cooling (Smyth 1974; Jackson et al. 2004), and here we have provided new evidence for the stability of OEN from high-pressure quenching. The depth at which the new OEN-HPCEN2 transition might occur in the upper mantle will depend on the Clapeyron slope of the transition, but our experiments suggest it as a viable candidate phase in the 300–400 km depth interval. Previous synthesis experiments suggest that the presence of shear stress and/or incorporation of hydrogen into MgSiO₃ pyroxene may stabilize the LPCEN and HPCEN *C2/c* structures, with the transition between the two taking place at shallower depths (Ulmer and Stadler 2001; Grover 1972; Jacobsen et al. 2010; Coe and Kirby 1975; Frost et al. 1978).

ACKNOWLEDGMENTS

This work was supported by the National Science Foundation (NSF) under Grant EAR07-38871. This work was also partially supported by the Consortium for Materials Properties Research in Earth Sciences (COMPRES) under NSF Cooperative Agreement EAR 10-43050. Portions of this work were performed at GSECARS (Sector 13), APS, Argonne National Laboratory. GSECARS is supported by the NSF Earth Sciences (EAR-0622171) and Department of Energy (DOE) and Geosciences (DE-FG02-94ER14466). Use of the Advanced Photon Source was supported by DOE under Contract No. DE-AC02-06CH11357. We thank Ian M. Steele for assistance with EMPA analysis, B. Reynard, R. Downs, C. Prewitt, and J. Smyth for helpful discussions. Reviews by J. Smyth and S. Jahn are appreciated and improved the manuscript.

REFERENCES CITED

- Akashi, A., Nishihara, Y., Takahashi, E., Nakajima, Y., Tange, Y., and Funakoshi, K. (2009) Orthoenstatite/clinoenstatite phase transformation in MgSiO₃ at high-pressure and high-temperature determined by in situ X-ray diffraction: Implications for nature of the X discontinuity. *Journal of Geophysical Research*, 114, B04206.
- Angel, R.J., Chopelas, A., and Ross, N.L. (1992) Stability of high-density clinoenstatite at upper-mantle pressures. *Nature*, 358, 322–324.
- Anthony, J.W., Bideaux, R.A., Bladh, K.W., and Nichols, M.C., Eds., *Handbook of Mineralogy*, Mineralogical Society of America, Chantilly, VA 20151-1110, USA. <http://www.handbookofmineralogy.org/>.
- Chopelas, A. (1999) Estimates of mantle relevant Clapeyron slopes in the MgSiO₃ system from high-pressure spectroscopic data. *American Mineralogist*, 84, 233–244.
- Coe, R.S. and Kirby, S.H. (1975) The orthoenstatite to clinoenstatite transformation by shearing and reversion by annealing: Mechanism and potential applications. *Contributions to Mineralogy and Petrology*, 52, 29–55.
- Crawford, A.J. (1980) A clinoenstatite-bearing cumulate olivine pyroxenite from Howqua, Victoria. *Contributions to Mineralogy and Petrology*, 75, 353–367.
- Dera, P. (2007) GSE_ADA data analysis program for monochromatic single-crystal diffraction with area detector. GSECARS, Chicago, Illinois.
- Deuss, A. and Woodhouse, J.H. (2004) The nature of the Lehmann discontinuity from its seismological Clapeyron slopes. *Earth and Planetary Science Letters*, 225, 295–304.
- Frost, B.R., Coe, R.S., and Okamura, F.P. (1978) Principal stress directions from a natural occurrence of stress-induced clinoenstatite. *Contributions to Mineralogy and Petrology*, 67, 116–129.
- Grandin de L'Épervier, A. and Ito, J. (1983) Flux growth of orthoenstatite by a multiple slow-cooling technique. *Journal of Crystal Growth*, 64, 411–412.
- Grover, J. (1972) The stability of low-clinoenstatite in the system Mg₂Si₂O₇-CaMgSi₂O₆ (abstract). *EOS Transactions, American Geophysical Union*, 53, 539.
- Hugh-Jones, D.A. and Angel, R.J. (1994) A compressional study of MgSiO₃ orthoenstatite up to 8.5 GPa. *American Mineralogist*, 79, 405–410.
- Ito, J. (1975) High temperature solvent growth of orthoenstatite MgSiO₃ in air. *Geophysical Research Letters*, 2, 533–536.
- Jackson, J.M., Sinogeikin, S.V., Carpenter, M.A., and Bass, J.D. (2004) Novel phase transition in orthoenstatite. *American Mineralogist*, 93, 239–245.
- Jacobsen, S.D., Liu, Z., Ballaran, T.B., Littlefield, E.F., Ehm, L., and Hemley, R.J. (2010) Effect of H₂O on upper mantle phase transitions in MgSiO₃: Is the depth of the seismic X-discontinuity an indicator of mantle water content? *Physics of the Earth and Planetary Interiors*, 183, 234–244.
- Jahn, S. (2008) High-pressure phase transitions in MgSiO₃ orthoenstatite studied by atomistic computer simulation. *American Mineralogist*, 93, 528–532.
- Kanzaki, M. (1991) Ortho/clinoenstatite transition. *Physics and Chemistry of Minerals*, 17, 726–730.
- Kung, J., Li, B., Uchida, T., Wang, Y., Neuville, D., and Liebermann, R.C. (2004) In situ measurements of sound velocities and densities across the orthopyroxene → high-pressure clinopyroxene transition in MgSiO₃ at high pressure. *Physics of Earth and Planetary Interiors*, 147, 27–44.
- Lin, C.-C. (2003) Pressure-induced metastable phase transition in orthoenstatite (MgSiO₃) at room temperature: A Raman spectroscopic study. *Journal of Solid State Chemistry*, 174, 403–411.
- (2004) Pressure-induced polymorphism in enstatite (MgSiO₃) at room temperature: Clinoenstatite and orthoenstatite. *Journal of Physics and Chemistry of Solids*, 65, 913–921.
- Mao, H.K., Xu, J., and Bell, P.M. (1986) Calibration of the ruby pressure gauge to 800 kbar under quasi-hydrostatic conditions. *Journal of Geophysical Research*, 91, 4673–4676.
- Morimoto, N., Appleman, D.E., and Evans, H.T. Jr. (1960) The crystal structures of clinoenstatite and pigeonite. *Zeitschrift für Kristallographie*, 114, 120–147.
- Morimoto, N. and Koto, K. (1969) The crystal structure of orthoenstatite. *Zeitschrift für Kristallographie*, 129, 65–83.
- Ohashi, H. (1984) Polysynthetically-twinning structures of enstatite and wollastonite. *Physics and Chemistry of Minerals*, 10, 217–229.
- Pacalo, R.E.G. and Gasparik, T. (1990) Reversals of the orthoenstatite-clinoenstatite transition at high pressures and high temperatures. *Journal of Geophysical Research*, 95, 15853.
- Papike, J.J., Prewitt, C.T., Sueno, S., and Cameron, M. (1973) Pyroxenes: Comparisons of real and ideal structural topologies. *Zeitschrift für Kristallographie*, 138, 254–273.
- Putz, H., Schon, J.C., and Jansen, M. (1999) Method for “ab initio” structure solution from powder diffraction data. *Journal of Applied Crystallography*, 32, 864–870.
- Rivers, M., Prakapenka, V.B., Kubo, A., Pullins, C., Holl, C.M., and Jacobsen, S.D. (2008) The COMPRES/GSECARS gas loading system for diamond anvil cells at the Advanced Photon Source. *High Pressure Research*, 28, 273–292.
- Sheldrick, G.M. (2008) A short history of SHELX. *Acta Crystallographica*, A64, 112–122.
- Shinmei, T., Tomioka, N., Fujino, K., Kuroda, K., and Irifune, T. (1999) In situ X-ray diffraction study of enstatite up to 12 GPa and 1473 K and equations of state. *American Mineralogist*, 84, 1588–1594.
- Shiraki, K., Kuroda, N., Urano, H., and Manuyama, S. (1980) Clinoenstatite in boninites from the Bonin Islands, Japan. *Nature*, 285, 31–32.
- Smyth, J. (1974) Experimental study on the polymorphism of enstatite. *American Mineralogist*, 59, 345–352.
- Thompson, R.M. and Downs, R.T. (2003) Model pyroxenes I: Ideal pyroxene topologies. *American Mineralogist*, 88, 653–666.
- Ulmer, P. and Stadler, R. (2001) The Mg(Fe)SiO₃ orthoenstatite-clinoenstatite transitions at high pressures and temperatures determined by Raman-spectroscopy on quenched samples. *American Mineralogist*, 86, 1267–1274.
- Woodland, A.B. (1998) The orthorhombic to high-P monoclinic phase transition in Mg-Fe pyroxenes: Can it produce a seismic discontinuity? *Geophysical Research Letters*, 25, 1241–1244.
- Yu, Y.G. and Wentzcovitch, R.M. (2009) Low-pressure clino- to high-pressure orthoenstatite phase transition: A phonon-related mechanism. *American Mineralogist*, 94, 461–466.

MANUSCRIPT RECEIVED DECEMBER 5, 2011

MANUSCRIPT ACCEPTED MARCH 26, 2012

MANUSCRIPT HANDLED BY SERGIO SPEZIALE